Supplemental material for: Critical Role of the Exchange Interaction for the Electronic Structure and Charge-Density-Wave Formation in $TiSe_2$

Below we present further details on the computational procedures, high-T phase crystal structure, phonon frequencies, PBE+U calculations, spin-orbit coupling and electronic structure compared to ARPES.

I. COMPUTATIONAL DETAILS

Results with PBE and PBE+U were obtained with Quantum ESPRESSO[1] and results with HSE06 with VASP[2,3] within the projector-augmented-wave (PAW) method.[4] A plane-wave cut-off of 320 eV was used and semi-core electrons were included in the Ti PAW potential. Results were converged with a $24 \times 24 \times 12$ k-point mesh in the high-T cell. For most calculations presented in the manuscript we used the all-electron `CRYSTAL` code[5] with an adapted molecular def2-TZVP basis set for solid state calculations. The results for the energy gain in HSE06 was within 1 meV/supercell in agreement between VASP and `CRYSTAL` (see Fig. 3 below).

II. HIGH-T PHASE CRYSTAL STRUCTURE

In Table I we present the experimental and theoretical lattice parameters and Se-z-positions of the high-T phase structure. The parameter a is the in-plane hexagonal lattice constant, c is the distance between layers and h is the distance between the Ti and Se layers. The hybrid functionals in combination with a simple Grimme D2[6] van der Waals correction give lattice parameters in good agreement with experiments. In our calculations we have, however, consistently used the experimental lattice parameters but relaxed atomic positions. Only the energy gain curves in Fig. 1 (b) of the manuscript were obtained with fixed Se-z-positions and fixed $\delta\mathrm{Ti}/\delta\mathrm{Se}(=3)$ ratio. At the minimum the atomic positions were again relaxed as described in the manuscript. In Fig. 1 we show the in-plane crystal structure in the high -and low-T phases. Big blue dots signifies Ti atoms and small green dots Se atoms. A dot on the Se atom indicates that the atom is on the opposite side of the Ti layer as compared to the Se atom without the dot. We have also replotted in a larger scale the p, d and $p-d$-hybridized orbitals of Fig. 3 (c) in the manuscript.

TABLE I. Lattice parameters are calculated within PBE, HSE06 and HSE(17,0). The van der Waals forces are accounted for via a Grimme D2[6] correction.

	Exp.[7]	PBE	HSE06	HSE(17,0)
a(Å)	3.540	3.519	3.528	3.531
c(Å)	6.007	6.130	6.104	6.113
h(Å)	1.532	1.555	1.522	1.527

III. PHONON FREQUENCIES IN THE HIGH-T PHASE

The phonon frequencies in the high-T phase are reported in Table II. In the high-T phase the phonons are measured at room temperature and thus cannot be calculated exactly within the harmonic approximation. Indeed, the two Raman active phonons at 200 $\mathrm{cm}^{-1}(\mathrm{A}_{1g})$ and at 136 cm^{-1} (E_g) are overestimated by hybrid functionals. It is expected that thermal effects would soften these values, and this trend was seen in experiment at least for the E_g mode in the high-T phase.[8] On the contrary, the IR active mode around 140 cm^{-1} is underestimated, with both HSE06 and HSE(17,0). This mode belongs to the same phonon branch as the soft mode at L which drives the instability and should thus harden significantly with temperature. Such behaviour can also be seen in experiment.[9]

TABLE II. Calculated zone center phonon frequencies (cm^{-1}) for the high-T structure compared with Raman (R) and Infrared (I) experiments.

Symm.	Exp.	PBE	HSE06	HSE(17,0)
E_g (R)	136[10] (273 K) / 134[11] (300 K)	136.9	147.5	147.3
E_u (I)	143[12] (300 K) /137[11] (300 K)	141.5	124.8	101.1
A_{1g} (R)	200[10] (273 K) /194[11] (300 K)	195.6	209.5	207.9
A_{2u}	-	292.7	323.8	314.4

IV. PHONON FREQUENCIES IN THE LOW-T PHASE

Tables III, IV and V report the computed Raman and infrared active frequencies in the CDW phase, comparing them to the peaks identified in several experimental spectra. They also contain an analysis of the CDW spectra in terms of back-folding of phonon modes from the Brillouin zone of the high-T phase. The q-points of the original lattice folded onto $\bar{\Gamma}$ in the supercell are Γ and A with weights 1, plus M and L with weights 3. By applying crystalline translations, all the phonon eigenvectors at $\bar{\Gamma}$ of the undistorted supercell are obtained from the phonon eigenvectors at the previously mentioned q-points of the unit cell. The degeneracy between frequencies at symmetry equivalent points is broken by the distortion, so that, e.g., the three degenerate modes from L_1, L_2 and L_3 split into an E and an A representation.

We label $|\sigma_{\mathbf{q}}\rangle$ the phonon eigenvectors at $\bar{\Gamma}$ of the high-T phase. $\mathbf{q}$ labels the q-point the mode is back-folded from. We then label $|\bar{\nu}\rangle$ the eigenvectors of the distorted low-T phase. We define the decomposition of a mode $|\bar{\nu}\rangle$ as the square overlap with the eigenvectors of the undistorted supercell $|\langle\bar{\nu}|\sigma_{\mathbf{q}}\rangle|^2$, and then sum over degenerate frequencies in the undistorted supercell. For any given $|\bar{\nu}\rangle$ we report in the tables the largest square overlaps as a function of σ (the ones larger than 10%), the frequency ω_σ and the point $\mathbf{q}$.

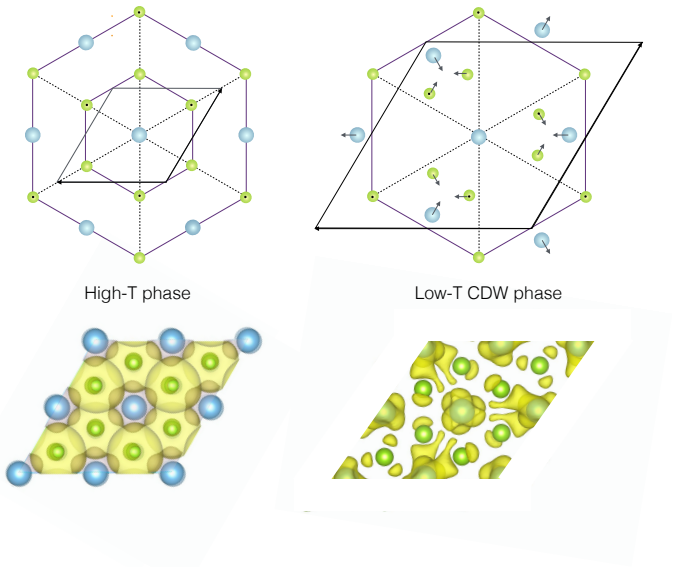

FIG. 1. In-plane crystal structure of the high -and low-T phases and the corresponding p, d and $p-d$-hybridized orbitals that participate in the CDW transition.

TABLE III. Raman peaks identified in experimental spectra of the CDW phase (at 53 K and 11K) compared to computed Raman active frequencies (cm^{-1}). The point(s) **q** in the Brillouin zone and the frequency(s) $\omega_{\text{undist.}}$ of the mode(s) of undistorted cell overlapping with the modes in the distorted cell are also reported, with the overlap percentage between parentheses. Only peaks identified as one phonon modes either in the experimental references or in this work are listed.

Symmetry	Exp.		Comment	Calc.			**q**	$\omega_{\text{undist.}}$
	53 K[11]	11K[10]		HSE(17,0)	HSE06	PBE		HSE06
E_g				30	31	28	A	28.3 (100)
E_g	74	78	CDW	80.3	72.6	55.9	L	-126 (95)
E_g	93	94		94.4	97.0	93.7	L	94.7 (97)
A_{1g}	116	119	CDW	126	114	96.8	L	-126 (75) + 117 (17)
E_g	114	115		115	118	111	L	117 (100)
A_{1g}		115		114	119	112	L	117 (83) + -126 (16)
E_g	136	138		136,139	141,144	132,135	A+M,$\Gamma + L$	133 (41)+152 (41) and 151 (50) +147 (35)
E_g	148		weak					
E_g				154	155	144	M+A	150 (53) + 133 (34)
E_g				154	157	148	Γ + L	147 (54) + 152 (39)
A_{1g}		151,158,163	weak					
A_{1g}	173	176		180	180	166	M	177.1 (94)
E_g				179	179	168	M+L+A	177 (72) + 205 (15) + 133 (10)
A_{1g}	187	195		200	202	187	M	204 (93)
E_g				201	203	189	M	204 (83) + 205 (12)
A_{1g}	204	206		215	214	199	Γ	210 (92)
E_g		212		217	215	202	L(80%) +M	207 (70) + 207 (12)
E_g	314	317		327	328	297	L	320 (99)

TABLE IV. Infrared phonons at obtained from reflectivity (ref.) and transmission (tr.) spectra. Peaks identified in infrared spectra of the CDW phase obtained from reflectivity (ref.) and transmission (tr.) experiments compared to computed infrared active frequencies of E_u symmetry. The point(s) **q** in the Brillouin zone of the mode(s) of undistorted cell overlapping with the modes in the distorted cell are also reported.

Exp. ref.		Exp. tr.		Comment	Calc.			**q**
18 K[12]	20 K[11]	28 K[9]	4 K[13]		HSE(17,0)	HSE06	PBE	
	42	40	37	weak				
	52	47	49	weak				
	64	64	64	weak				
	76	74	72	CDW	73.3	67.5	66	M
	90	88	100	weak	102	105	100	M
118.2	118	118	118	weak	119	123	115	M
139.5	137	139	140		137,138	141,143	132,137	Γ+L,A+M
151.3	152	152	153		152,155	154,156	143,150	M+A,L+Γ
	162	166	164	weak				
171.9	175	176	173		176	177	167	L+M
	178		186	weak				
196.9	198	198	198		203	205	192	L+M
213.0		214	211		219	217	205	M+L
			222					
		230	234					
		280						
		315			330	333	305	M

TABLE V. Computed infrared active frequencies with the point(s) **q** in the Brillouin zone and the frequency(s) $\omega_{\text{undist.}}$ of the mode(s) of undistorted cell overlapping with the modes in the distorted cell. The overlap percentage is reported between parentheses.

Symmetry	HSE(17,0)	PBE	HSE06	**q**	$\omega_{\text{undist.}}$ HSE06
E_u	73.3	66.1	78.9	M	-100 (96)
A_{2u}	101	99.7	105	M	102 (92)
E_u	102	100	106	M	102 (96)
E_u	119	115	123	M	122 (99)
E_u	137	132	141	Γ+L	124 (60) + 152 (30)
E_u	138	136	143	A+M	149 (60) + 147 (30)
A_{2u}	143	137	150	L+M	152 (74) + 147 (25)
A_{2u}	146	139	151	M+L	147 (71) + 152 (26)
E_u	152	143	155	M+A	147 (62) + 149 (33)
E_u	155	150	158	L+Γ	152 (68) +124 (24)
E_u	176	167	177	L+M	176 (75) + 207 (12)
E_u	203	192	206	L+M	207 (78) + 207 (16)
A_{2u}	202	197	208	M	207 (98)
E_u	219	205	218	M+L	207 (76) + 207 (15)
A_{2u}	320	296	328	Γ+M	323 (69) + 329 (30)
A_{2u}	326	301	332	M+Γ	329 (69) + 323 (30)
E_u	330	305	334	M	329 (99)

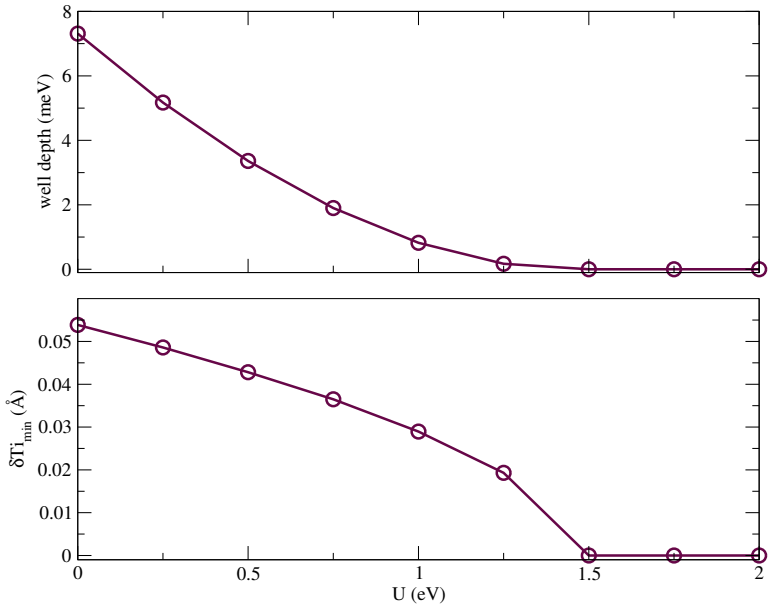

FIG. 2. The upper panel shows the absolute energy gain or well-depth as a function of U within PBE+U and the lower panel shows the corresponding displacement $\delta\mathrm{Ti}_{\mathrm{min}}$.

V. CDW INSTABILITY AS A FUNCTION OF U

In Fig. 2 we present the energy gain in the CDW distortion obtained with the PBE+U method for values of U between 0 to 2 eV. We see that the energy gain reduces monotonically with U and vanishes at 1.5 eV. This can be compared to the LDA+U result of U=2.5 eV in Ref. 14. The PBE+U band-structure agrees well with HSE06 at U=3.25 eV. The corresponding value in LDA+U is 3.5 eV.

VI. SPIN-ORBIT COUPLING

The calculations presented in the main paper were obtained without spin-orbit coupling (SOC). We did, however, also perform calculations including SOC (using VASP since SOC is not an available option in `CRYSTAL`). We verified that SOC only added a minor quantitative correction and did not change the qualitative analysis. Including SOC increases the computational cost substantially and we could therefore only carry out a limited number of calculations. Furthermore, to make the calculations feasible we had to omit the $3p$ semi-core electrons in the Ti pseudo potential. This increases the energy gain but is not expected to change the effect of SOC, since SOC influences mainly the Se bands. The semi-core electrons are also not expected to largely influence the electron-phonon coupling (EPC) of the high-T phase. Indeed, we found a difference in the EPC of only 4%. In Fig. 3 we have summarised our analysis using HSE06. At large displacement δTi, the energy gain is around twice as large when omitting semi-core electrons. The effect is smaller, the smaller is the distortion, consistent with the fact that both the band structure and the EPC are very similar with and without semi-core electrons.

Including SOC we find only a very small change, the maximum being 2 meV at the minimum of the curve. At small distortion the difference is vanishingly small. The effect of SOC reduces the EPC in HSE06 from $19\,\mathrm{eV}^2/\mathrm{Å}^2$ to $16\,\mathrm{eV}^2/\mathrm{Å}^2$, which is compensated by the change in band structure. Apart from the indirect effect of SOC on the orbitals and the self-consistent potential there is a direct effect due to extra SOC terms in the Hamiltonian.[15] Since these terms are semi-local and density independent, we expect them to give only a small contribution to the non-local $p-d$ EPC and to be the same for all HSE functionals having the same band structure. The indirect effect is also expected to be small and similar for all HSE functionals. Indeed, similarly to HSE06, a reduction of approximately $3\,\mathrm{eV}^2/\mathrm{Å}^2$ is found for HSE(30,0.3), which is accompanied by an identical change in band structure, and no difference in energy gain. We therefore expect that the relative EPC strengths with SOC and non local functionals are qualitatively the same as those found without SOC.

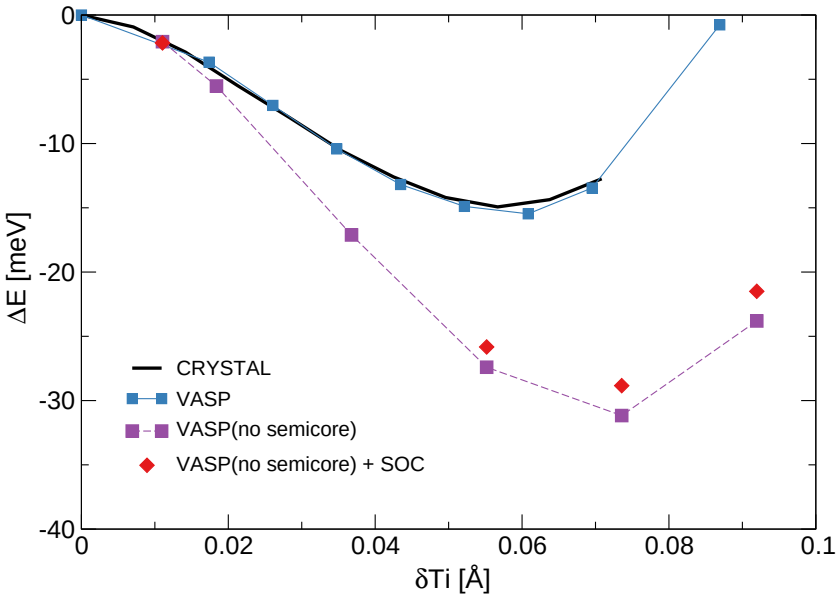

FIG. 3. Energy gain within HSE06 calculated with `CRYSTAL` and VASP. We compare results with and without semi-core electrons in the Ti-PAW potential, and with and without SOC.

VII. ELECTRONIC STRUCTURE COMPARED TO ARPES

In order to compare the band structure with experiment it is important to take into account the Se-p band splitting around Γ in the high-T phase which is due to SOC.[16] In Fig. 4 we report calculated band structures in the high (a) -and low-T (b) phases superimposed on ARPES measurements by Rohwer et al..[17] In the high-T phase we calculated the bands along $M'-\Gamma-M$ (black), $L'-\Gamma-L$ (orange) and along a line in between with $k_z = 0.33$ (red). The band dispersions are well-reproduced and the band overlap ($\Gamma - L$) is only slightly overestimated with HSE06. The bands in the CDW phase are calculated at the minimum of the curve in Fig. 1b of the manuscript and we note that band gap is indirect between Γ and A. The gaps in HSE06 and HSE(17,0) are 0.21 eV and 0.35 eV, respectively. Both are somewhat overestimated compared to the experimental value which has been estimated to 0.15 eV.

[1] P. Giannozzi *et al*, J. Phys.: Condens. Matter **21**, 395502 (2009).
[2] G. Kresse and J. Furthmüller, Phys. Rev. B **54**, 11169 (1996).
[3] G. Kresse and J. Furthmüller, Comput. Mater. Sci. **6**, 15 (1996).
[4] G. Kresse and D. Joubert, Phys. Rev. B **59**, 1758 (1999).
[5] R. Dovesi, R. Orlando, A. Erba, C. M. Zicovich-Wilson, B. Civalleri, S. Casassa, L. Maschio, M. Ferrabone, M. D. L. Pierre, P. Darco, Y. Noel, M. Causa, M. Rerat, and B. Kirtman, Int. J. Quantum Chem. **114**, 1287 (2014).
[6] S. Grimme, Journal of Computational Chemistry **27**, 1787 (2006).
[7] C. Riekel, Journal of Solid State Chemistry **17**, 389 (1976).
[8] D. L. Duong, G. Ryu, A. Hoyer, C. Lin, M. Burghard, and K. Kern, ACS Nano **11**, 1034 (2017).
[9] S. Uchida and S. Sugai, Physica B+C **105**, 393 (1981).
[10] S. Sugai, K. Murase, S. Uchida, and S. Tanaka, Solid State Communications **35**, 433 (1980).
[11] J. A. Holy, K. C. Woo, M. V. Klein, and F. C. Brown, Phys. Rev. B **16**, 3628 (1977).
[12] W. Y. Liang, G. Lucovsky, J. C. Mikkelsen, and R. H. Friend, Philosophical Magazine Part B **39**, 133 (1979).
[13] J. A. Wilson, physica status solidi (b) **86**, 11 (1978).
[14] R. Bianco, M. Calandra, and F. Mauri, Phys. Rev. B **92**, 094107 (2015).
[15] M. J. Verstraete, M. Torrent, F. Jollet, G. Zérah, and X. Gonze, Phys. Rev. B **78**, 045119 (2008).
[16] Z. Vydrova, E. F. Schwier, G. Monney, T. Jaouen, E. Razzoli, C. Monney, B. Hildebrand, C. Didiot, H. Berger, T. Schmitt, V. N. Strocov, F. Vanini, and P. Aebi, Phys. Rev. B **91**, 235129 (2015).
[17] T. Rohwer, S. Hellmann, M. Wiesenmayer, C. Sohrt, A. Stange, B. Slomski, A. Carr, Y. Liu, L. M. Avila, M. Kallane, S. Mathias, L. Kipp, K. Rossnagel, and M. Bauer, Nature **471**, 490 (2011).

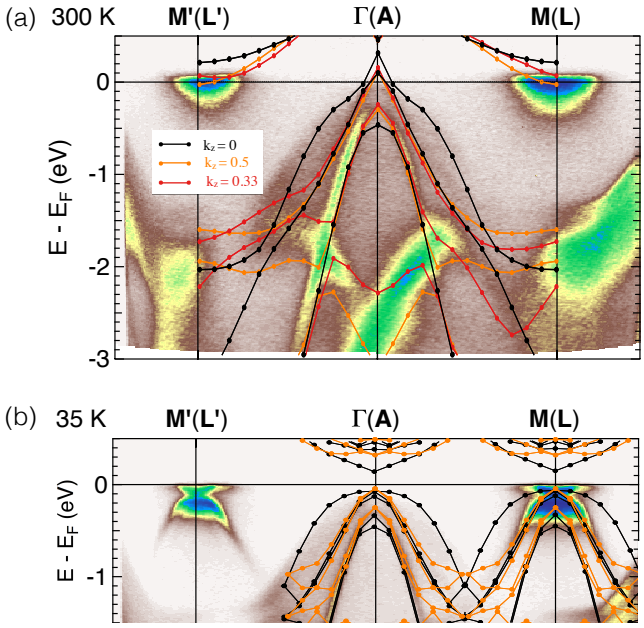

FIG. 4. HSE06 electronic structure of the high (a) and low-T phases (b) compared to ARPES. k_z values are given in units of $2\pi/c$.